Experimental and Theoretical Studies of the Basicity and Proton Affinity of SiF_4 and the Structure of SiF_4H^+

Yun Ling, Rebecca K. Milburn, Alan C. Hopkinson, and Diethard K. Bohme*

Department of Chemistry and Centre for Research in Earth and Space Science, York University, Toronto, Ontario, Canada

A combined experimental and theoretical approach has been employed to establish the basicity and proton affinity of SiF_4 and the structure of SiF_4H^+. The kinetics and energetics for the transfer of a proton between SiF_4, N_2, and Xe have been explored experimentally in helium at 0.35 ± 0.02 torr and 297 ± 3 K with a selected-ion flow tube apparatus. The results of equilibrium constant measurements are reported that provide a basicity and proton affinity for SiF_4 at 297 ± 3 K of 111.4 ± 1.0 and 117.7 ± 1.2 kcal mol^{-1}, respectively. These values are more than 2.5 kcal mol^{-1} lower than currently recommended values. The basicity order was determined to be GB(Xe) > GB(SiF_4) > GB(N_2), while the proton-affinity order was shown to be PA(Xe) > PA(N_2) > PA (SiF_4). Ab initio molecular orbital computations at MP4SDTQ(fc)/6-311++G(3df,3pd) using geometries from B3LYP/6-31+G(d,p) indicate a value for PA(SiF_4) = 118.7 kcal mol^{-1} that is in good agreement with experiment. Also, the most stable structure of SiF_4H^+ is shown to correspond to a core SiF_3^+ cation solvated by HF with a binding energy of 43.9 kcal mol^{-1}. Support for this structure is found in separate SIFT collision induced dissociation (CID) measurements that indicate exclusive loss of HF. (J Am Soc Mass Spectrom 1999, 10, 848–855) © 1999 American Society for Mass Spectrometry

The gas-phase protonation of SiF_4 was first reported in 1983 as part of tandem mass spectrometer measurements of ion–molecule reactions occurring in mixtures of silicon tetrafluoride and deuterium [1]. These early studies were initiated in part to elucidate the mechanism of the plasma-induced decomposition of SiF_4–H_2 mixtures. The observed protonation was a consequence of the reaction of D_3^+ with SiF_4 [1]. The first, and to our knowledge only, determination of the proton affinity of SiF_4 was reported shortly thereafter in 1984 [2]. Specifically, Fourier-transform mass spectrometer (FTMS) measurements of the proton-transfer equilibrium (1) provided a value for PA(SiF_4) = 116 kcal mol^{-1},

$$SiF_4H^+ + N_2 \leftrightharpoons N_2H^+ + SiF_4 \quad (1)$$

that is 2 kcal mol^{-1} higher than the value for PA(N_2) = 114 kcal mol^{-1} which was used as a reference. However, details on the measured equilibrium constant and the standard entropy change required to calculate ΔPA from the standard free-energy change for reaction 1 were not reported [2]. Current tabulations of proton affinities recommend a value for PA(SiF_4) of 120.2 kcal mol^{-1} with PA(N_2) = 118.2 and 118.0 kcal mol^{-1} [3, 4] and PA(Xe) = 118.6 and 119.4 kcal mol^{-1} [3, 4].

We report here results of a combined experimental and theoretical study that provides an improved value for PA(SiF_4) and also corrects the currently tabulated relative affinities for the transfer of a proton between SiF_4, N_2, and Xe.

$$SiF_4H^+ + Xe \leftrightharpoons XeH^+ + SiF_4 \quad (2)$$

$$N_2H^+ + Xe \leftrightharpoons XeH^+ + N_2 \quad (3)$$

The experiments were directed at equilibrium-constant measurements for reactions 1, 2, and 3 using the selected-ion flow tube (SIFT) technique. The measurements for reaction 3 were performed to assess internal consistency. The equilibrium constant for this reaction has been well established previously with measurements using the flowing-afterglow technique [5] and a standard free-energy change has been determined using high-pressure mass spectrometry [6].

The experimental studies are complemented with state-of-the-art ab initio molecular orbital computations at various high levels of theory. The computations are directed toward the evaluation of PA(SiF_4) and the energy and structure of SiF_4H^+. Finally, selected-ion

Address reprint requests to Dr. Diethard K. Bohme, Dept. of Chemistry, York University, 4700 Keele St., Toronto, Ontario M3J 1P3, Canada.

Dedicated in memory of Bob Squires, in part for his outstanding contributions to the thermochemistry of ions.

1044-0305/99/$20.00
PII S1044-0305(99)00045-8

Received November 30, 1998
Revised February 22, 1999
Accepted February 22, 1999

Table 1. Product distributions and rate coefficients measured with the SIFT technique for reactions of SiF_4H^+ and SiF_4 in He at 297 ± 3 K and 0.35 ± 0.02 torr

Reactants	Products	BR[a]	k_{obs}[b]	k_{cap}[c]	RE[d]
$SiF_4H^+ + Xe$	$XeH^+ + SiF_4$	>0.98	5.1	6.2	0.82
	$SiF_3Xe^+ + HF$	<0.02			
$SiF_4H^+ + N_2$	$N_2H^+ + SiF_4$	0.80	2.0	6.6	0.30
	$SiF_4N_2H^+$	0.14			
	$SiF_3N_2^+ + HF$	0.06			
$N_2H^+ + SiF_4$	$SiF_4H^+ + N_2$	0.74	3.8	11.5	0.33
	$SiF_3^+ + HF + N_2$	0.13			
	$SiF_4N_2H^+$	0.10			
	$SiF_3N_2^+ + HF$	0.03			
$SiF_4H^+ + SiF_4$	$(SiF_4)_2H^+$		2.2		
$SiF_3^+ + SiF_4$	$Si_2F_7^+$		5.7	8.0	0.71
$SiF_3N_2^+ + SiF_4$	$Si_2F_7^+ + N_2$		3.4	7.4	0.46

[a]Reaction branching ratio.
[b]Observed apparent bimolecular rate coefficient in units of 10^{-10} cm^3 $molecule^{-1}$ s^{-1} with an uncertainty of ±30%.
[c]Theoretical capture rate coefficient in units of 10^{-10} cm^3 $molecule^{-1}$ s^{-1} calculated with the Langevin theory [21].
[d]Reaction efficiency, RE, expressed as a ratio of the experimental rate coefficient, to the theoretical capture rate coefficient, k_{obs}/k_{cap}.

flow tube collision induced dissociation (SIFT-CID) experiments were performed to provide some experimental insight into the structure of SiF_4H^+.

Experimental

Measurements of rate coefficients and equilibrium constants were performed with the SIFT technique in the Ion Chemistry Laboratory at York University [7–9]. In studies of reactions 1 and 2, SiF_4H^+ was established upstream in the flow tube by the following sequence of ion–molecule reactions:

$$Ar^+ + H_2 \rightarrow ArH^+ + H \quad (4)$$

$$ArH^+ + H_2 \rightarrow H_3^+ + Ar \quad (5)$$

$$H_3^+ + SiF_4 \rightarrow SiF_4H^+ + H_2 \quad (6)$$

The Ar^+ was formed by electron impact on Ar (Air Products Canada, 99.998%) within a low-pressure ion source, mass selected and introduced via a Venturi inlet into a flow of He buffer at a pressure of 0.35 ± 0.02 torr. H_2 (Matheson, 99.99% min) and SiF_4 (Matheson, > 99.6 mol %) were added sequentially upstream of the reaction region. The proton-transfer reactions of SiF_4H^+ with Xe and N_2 were investigated by adding Xe (Matheson, 99.995% min.) or N_2 (Air Products Canada, 99.998%) into the reaction region downstream. In studies of reaction 3 N_2H^+ was established as a dominant ion upstream of the reaction region by reacting H_3^+ with N_2 according to reaction 7.

$$H_3^+ + N_2 \rightarrow N_2H^+ + H_2 \quad (7)$$

Rate coefficients and equilibrium constants were determined in the usual manner. The equilibrium constant K was obtained from both the ratio of the forward to reverse rate coefficients, k_f/k_r, and from equilibrium ion concentrations. Briefly, the forward and reverse rate coefficients were determined by fitting the decay of the reactant ion with the solution of the differential rate equation for a reversible reaction. Also, the product to reactant ion–signal ratio was plotted against the flow of the neutral forward reactant for various different flows of the reverse reactant. The equilibrium constant, K_e, is determined by the slope of the linear portion at high flows once equilibrium is achieved [9].

Bond connectivities within SiF_4H^+ were investigated with multi-CID experiments by raising the sampling nose-cone voltage from 0 to −80 V while concomitantly varying the potential of front and rear quadrupole focusing lenses so as not to introduce mass discrimination [10].

Theoretical

Standard ab initio molecular orbital calculations were performed using the GAUSSIAN 94 program [11]. The density functional Becke three parameter hybrid method [12a–m] that includes the Slater (local spin density) exchange functional [12a,b, 13] with nonlocal gradient-corrected terms [14] and the Lee–Yang–Parr method which includes local and nonlocal gradient corrected correlation functionals, denoted B3LYP, was used to optimize geometries [15, 16]. This method with a basis set of 6-31+G(d,p) [17] will be denoted as B3LYP/6-31+G(d,p). The optimized geometries at B3LYP/6-31+G(d,p) were characterized by harmonic frequency calculations and these showed all structures to be at minima. The frequency calculations also yielded the zero-point energies, which were left unscaled, and thermal corrections. Single-point calculations were done at fourth-order Møller–Plesset [18] theory with a frozen core, using two different basis sets, 6-311++G(2df,p) [19] and 6-311++G(3df,3pd) with geometries from B3LYP/6-31+G(d,p) optimizations. These calculations will be abbreviated to MP4(2df,p) and MP4(3df,3pd) respectively. Single-point calculations with a frozen core were also performed at the QCISD(T) level [20] with a basis set of 6-311++G(3df,3pd), again using

Table 2. Summary of experimental equilibrium results at 297 ± 3 K for proton-transfer reactions, $B_1H^+ + B_2 \leftrightharpoons B_2H^+ + B_1$

B_1	B_2	$(k_f/k_r)^a$	$K_e{}^b$	K[c]
N_2	Xe	53 ± 13	55 ± 11	54.1 ± 8.4
SiF_4	Xe	25.3 ± 4.1	23.4 ± 4.2	24.4 ± 2.9
SiF_4	N_2	0.59 ± 0.15	0.56 ± 0.11	0.57 ± 0.09

[a]Obtained from a fit to the decay of B_1H^+.
[b]Obtained from an ion-signal ratio plot.
[c]Best estimate of the equilibrium constant.

the geometries optimized at B3LYP/6-31+G(d,p). Using Pople's notation, this is denoted as QCISD(T)(fc)/6-311++G(3df,3pd)//B3LYP/6-31+G(d,p), which we abbreviate to QCI(3df,3pd).

Results and Discussion

The results of the rate-coefficient and equilibrium-constant measurements are summarized in Tables 1 and 2.

$N_2H^+ + Xe$

Measurements of the approach to, and attainment of, equilibrium for reaction 3 were straightforward. A ratio of rate coefficients, $k_3/k_{-3} = 53 \pm 13$, was determined from a fit to the decay of the N_2H^+ signal and equilibrium–ion ratio plots provided a value for $K_3 = 55 \pm 11$. The best estimate of the equilibrium constant for reaction 3 is therefore 54 ± 8, which is in good agreement with the best estimate of 58 ± 8 determined previously (using both methods) with the flowing-afterglow technique [5].

$SiF_4H^+ + Xe$

Figure 1 displays results of measurements for the proton-transfer reaction 2. Not shown in Figure 1 is the production of trace quantities (2%) of SiF_3Xe^+. The origin of this ion is not certain. It may arise from the HF-elimination reaction 8 that has been reported to occur in trace amounts in a Fourier-transform ion-cyclotron resonance (FT-ICR) spectrometer [22].

$$SiF_4H^+ + Xe \leftrightharpoons SiF_3Xe^+ + HF \quad (8)$$

Another possible source is the addition reaction 9

$$SiF_3^+ + Xe + He \rightarrow SiF_3Xe^+ + He \quad (9)$$

that we have shown in separate experiments to occur under similar SIFT conditions with a rate coefficient $k_9 > 1 \times 10^{-11}$ cm^3 molecule^{-1} s^{-1}. Trace amounts of SiF_3^+ (1%), also not shown in Figure 1, were observed among the initial ions shown in Figure 1 (top).

The decay of SiF_4H^+ shown in Figure 1 (top) is accompanied by an increase in the XeH^+ signal. The curvature in the SiF_4H^+ decay with increasing Xe flow can be attributed to the occurrence of the reverse of reaction 2. Curve fitting of this decay in three separate experiments over a range of SiF_4 flows from 1.0×10^{18} to 1.9×10^{18} molecules s^{-1} provided a mean value for the ratio of rate constants, $k_2/k_{-2} = 25.3 \pm 4.1$. Also shown in Figure 1 (bottom) is a plot of the ratio of the XeH^+ to the SiF_4H^+ signal (corrected for mass discrimination) as a function of the Xe flow. The slope of the line affords a direct determination of the equilibrium

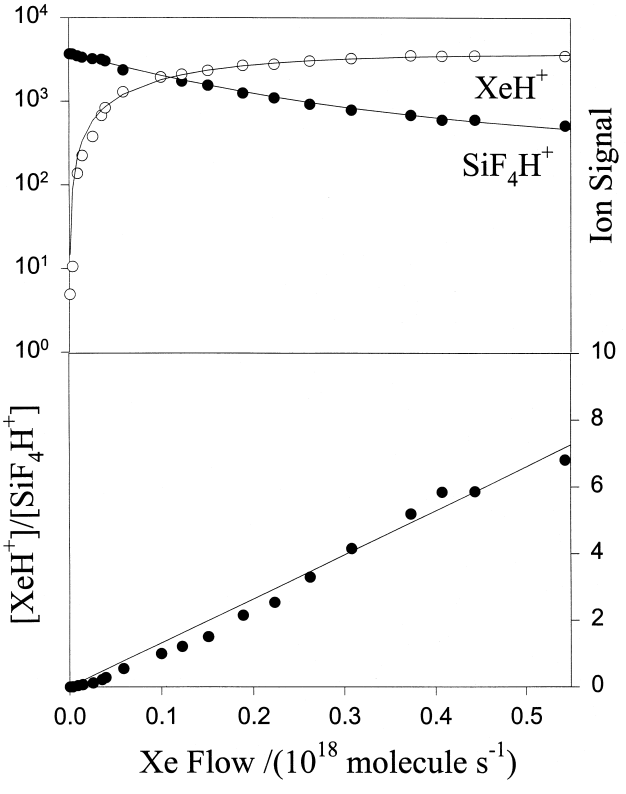

Figure 1. Top: Ion signal intensities vs Xe flow rate monitored for the reaction of SiF_4H^+ with Xe at a flow rate of SiF_4 = (1.9 ± 0.3) × 10^{18} molecules s^{-1}. The solid and open points represent experimental data. Only the largest isotope of XeH^+ was monitored; the XeH^+ signal shown has been corrected for the contribution of the other isotopes. The solid line for SiF_4H^+ is the computer fit used to determine the forward and reverse rate coefficients. T = 297 ± 3 K, P = 0.35 ± 0.02 torr. Bottom: The observed variation in $[XeH^+]/[SiF_4H^+]$ with Xe flow rate showing the approach to and attainment of equilibrium for the reaction $SiF_4H^+ + Xe = XeH^+ + SiF_4$ at a SiF_4 flow = (1.9 ± 0.3) × 10^{18} molecules s^{-1}. The best straight line through the experimental data points at high Xe flow yields a value for the equilibrium constant K = 25.1. T = 297 ± 3 K, P = 0.35 ± 0.02 torr.

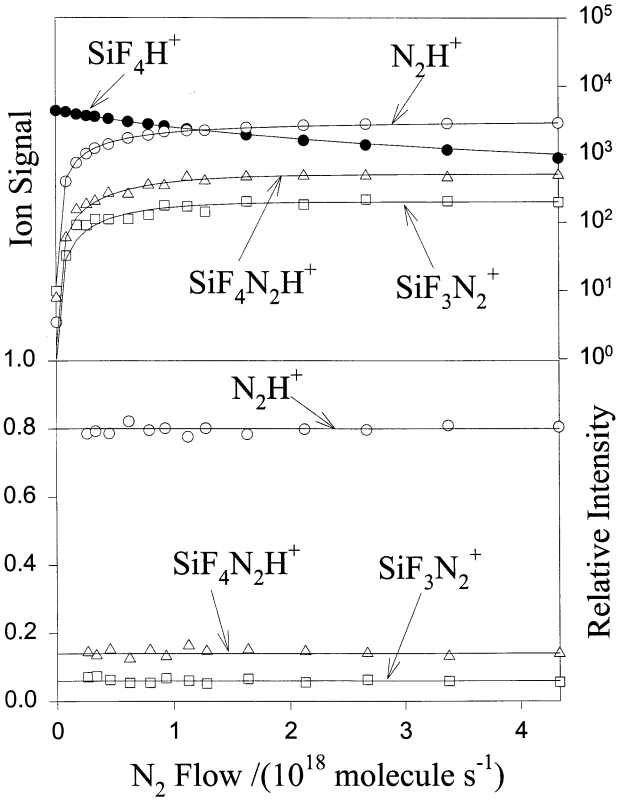

Figure 2. Top: Variations in the reactant and product ion signals monitored for the reaction of SiF_4H^+ with N_2 at a flow rate of SiF_4 = (7.5 ± 0.9) × 10^{17} molecules s^{-1}. Bottom: A plot of the relative intensity of the product ions vs flow. T = 297 ± 3 K, P = 0.35 ± 0.02 torr.

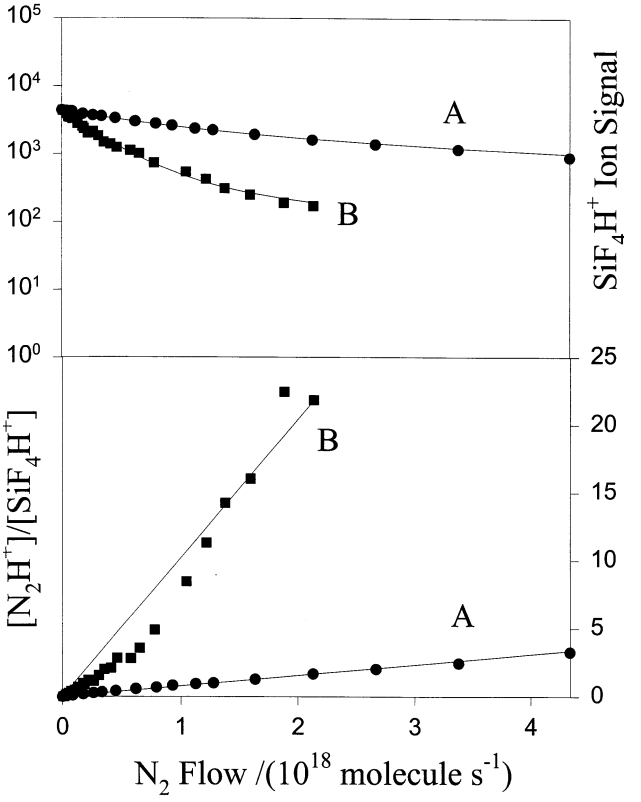

Figure 3. Top: Variations in the SiF_4H^+ signal as a function of N_2 flow for the reaction of $SiF_4H^+ + N_2 = N_2H^+ + SiF_4$ at two different additions of SiF_4 (A = 7.5 and B = 0.53 × 10^{17} molecules s^{-1}). The solid points represent experimental data and the solid lines are computer fits used to determine the forward and reverse rate coefficients. Bottom: Observed variations in $[N_2H^+]/[SiF_4H^+]$ as a function of N_2 flow rate for the same two SiF_4 additions. The slopes of the straight lines through the experimental data points are proportional to the equilibrium constant. An approach to equilibrium is evident at the lower flow of SiF_4 (curve B). T = 297 ± 3 K, P = 0.35 ± 0.02 torr.

constant from equilibrium concentrations. The three experiments yielded a mean value for K_2 = 23.4 ± 4.2, which is in agreement, within experimental error, with the value for k_2/k_{-2} determined with the fitting procedure.

$SiF_4H^+ + N_2$

Figure 2 (top) shows data obtained for reaction 1. Two minor reaction channels in addition to proton transfer were observed. Figure 2 (bottom) shows the determination of the branching fractions for these two channels. They correspond to addition (14%), presumably due to the termolecular association reaction 10, to form what may be a proton-bound adduct, $SiF_4 \cdot\cdot H^+ \cdot\cdot N_2$, or solvated SiF_3^+, $N_2 \cdot\cdot SiF_3^+ \cdot\cdot FH$, and the bimolecular elimination of HF (6%) according to reaction 11.

$$SiF_4H^+ + N_2 + He \rightarrow SiF_4N_2H^+ + He \quad (10)$$

$$SiF_4H^+ + N_2 \rightarrow SiF_3N_2^+ + HF \quad (11)$$

Figure 3 (top) shows the observed decline of an SiF_4H^+ signal with increasing N_2 addition at two different flows of SiF_4. The curvature in this decline is due to the occurrence of the reverse of reaction 1. Fitting this curvature provided a value for k_1/k_{-1} = 0.59 ± 0.15. This value is less than 1 so that the preferred direction of proton transfer is the reverse of reaction 1. The equilibrium constant determined from the ion signal ratio plots [see Figure 3 (bottom)], was K_1 = 0.56 ± 0.11, which is in good agreement with the value determined for k_1/k_{-1}.

$N_2H^+ + SiF_4$

Data obtained from a study of the reverse of reaction 1 is shown in Figure 4. N_2H^+ in this case was generated from the reaction of $N_2^+ + H_2$. Several other channels were again observed to compete with the transfer of a proton. This is indicated in reaction 12. The measured branching ratio is $a/b/c/d$ = 0.74/0.13/0.10/0.03.

$$N_2H^+ + SiF_4 \rightarrow SiF_4H^+ + N_2 \quad (12a)$$

$$N_2H^+ + SiF_4 \rightarrow SiF_3^+ + HF + N_2 \quad (12b)$$

$$N_2H^+ + SiF_4 + He \rightarrow SiF_4N_2H^+ \quad (12c)$$

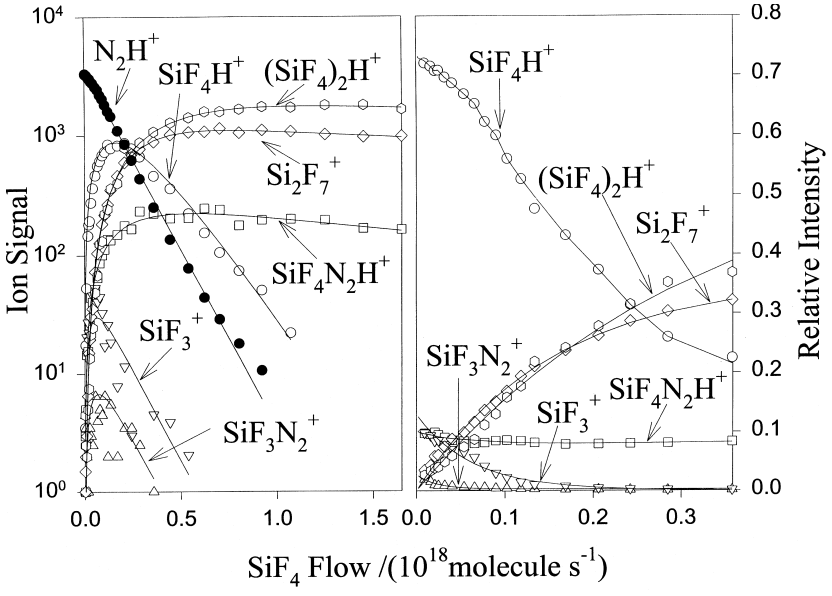

Figure 4. Left: Variations in the reactant and product ion signals monitored for the reaction of N_2H^+ with SiF_4. N_2H^+ is produced from the reaction of N_2^+ with H_2. Right: A plot of the relative intensity of the product ions vs. flow. $T = 297 \pm 3$ K, $P = 0.35 \pm 0.02$ torr.

$$N_2H^+ + SiF_4 \rightarrow SiF_3N_2^+ + HF \quad (12d)$$

The total rate coefficient for this reaction measured from the decline in the N_2H^+ signal was 3.8×10^{-10} cm^3 $molecule^{-1}$ s^{-1}. Also, a fast secondary reaction, reaction 13a,

$$SiF_4H^+ + SiF_4 + He \rightarrow (SiF_4)_2H^+ + He \quad (13a)$$

$$SiF_4H^+ + SiF_4 \rightarrow Si_2F_7^+ + HF \quad (13b)$$

leading to the formation of what is likely to be the protonated dimer of SiF_4 and to the $Si_2F_7^+$ ion was observed to compete with the reverse proton transfer and so prevent the attainment of equilibrium. Nevertheless, the ratio of rate coefficients, $k_1/k_{12a} = 0.57$, is consistent with the equilibrium results obtained from the study of the forward direction of reaction 1. An effective bimolecular rate coefficient of 2.2×10^{-10} cm^3 $molecule^{-1}$ s^{-1} was obtained for reaction 13 by fitting the rise and fall of the SiF_4H^+ signal in Figure 4. The secondary reactions 14 and 15 also contribute to the formation of $Si_2F_7^+$.

$$SiF_3^+ + SiF_4 + He \rightarrow Si_2F_7^+ + He \quad (14)$$

$$SiF_3N_2^+ + SiF_4 \rightarrow Si_2F_7^+ + N_2 \quad (15)$$

This was demonstrated in separate experiments in which SiF_3^+ and $SiF_3N_2^+$ were established as dominant primary ions. The rate coefficients measured for these reactions are 5.7×10^{-10} and 3.4×10^{-10} cm^3 $molecule^{-1}$ s^{-1}, respectively. The nature of the bonding in $SiF_3N_2^+$ is intriguing. This ion previously has been observed to be formed by the bimolecular reactions of SiF_4^+ with N_2 [2] and of N_2^+ with SiF_4 [2, 23a]. Also, $SiF_3N_2^+$ has been suggested to have the structure of an adduct ion, SiF_3^+–N_2, in which the interaction between the SiF_3^+ and N_2 is stronger than in SiF_3^+–F because N_2 has higher polarizability than the F atom [23a]. The bond dissociation energy for SiF_3^+-F was measured to be only 21.3 ± 1.5 kcal mol^{-1} by Armentrout et al. [23b].

Gas-Phase Basicities

The measured equilibrium constants for the proton-transfer reactions 1–3 are summarized in Table 2. There is good internal consistency because $K_1 = 0.57 \pm 0.09$ is equal to $K_2/K_3 = 0.45 \pm 0.12$. Table 3 summarizes the values for the overall standard free energy changes of the proton-transfer reactions 1–3 determined from

Table 3. Derived thermochemical data at 298 K for proton transfer reactions, $B_1H^+ + B_2 \leftrightharpoons B_2H^+ + B_1$

B_1	B_2	ΔG^0 (kcal mol^{-1})	ΔS^{0a} (cal mol^{-1} K^{-1})	ΔH^0 (kcal mol^{-1})
N_2	Xe	-2.36 ± 0.10	6.3	-0.48 ± 0.10
SiF_4	Xe	-1.89 ± 0.07	3.9	-0.73 ± 0.07
SiF_4	N_2	0.33 ± 0.09	-2.4	-0.38 ± 0.09

[a]Calculated from the standard entropies of the corresponding half reactions, $\Delta S^0_{1/2}$ for $B \rightarrow BH^+$ [4].

Table 4. Total energies (in hartrees) and zero-point and thermal energies (both in kcal mol^{-1})

	B3LYP[a]	ZPE[b]	Thermal[c]	MP4(2df,p)[d]	QCI(3df,3pd)[e]	MP4(3df,3pd)[f]
SiF_3^+	−588.80365	6.0	2.6	−588.06310	−588.07399	−588.08111
SiF_4	−689.10852	8.0	3.1	−688.26853	−688.28410	−688.29151
SiF_4H^+ (eclipsed)	−689.31181	13.7	3.9	−688.46042	−688.48125	−688.48859
SiF_4H^+ (staggered)	−689.31148[g]	13.5	3.5	—	—	—
HF	−100.42746	5.8	1.5	−100.33124	−100.34157	−100.33483
Si (triplet)	−289.37173	—	—	−288.92623	−288.92815	−288.92693
F	−99.71553	—	—	−99.61423	−99.61780	−99.61814
H	−0.50027	—	—	−0.49982	−0.49982	−0.49982
H_2	−1.17854	—	—	−1.16777	−1.17253	−1.17192

[a]Geometry optimization at B3LYP/6-31+G(d,p).
[b]Zero-point energies from B3LYP/6-31+G(d,p) optimization, unscaled.
[c]Thermal corrections from B3LYP/6-31+G(d,p) optimization.
[d]Single-point calculation at MP4SDTQ(fc)/6-311++G(2df,p) using geometries from B3LYP/6-31+G(d,p).
[e]Single-point calculation at QCISD(T)(fc)/6-311++G(3df,3pd) using geometries from B3LYP/6-31+G(d,p).
[f]Single-point calculation at MP4SDTQ(fc)/6-311++G(3df,3pd) using geometries from B3LYP/6-31+G(d,p).
[g]Transition state.

the relationship $\Delta G^0 = -RT \ln K$. $\Delta G^0(3) = -2.36 \pm 0.10$ kcal mol^{-1} determined in this study agrees with the value of -2.4 ± 0.1 kcal mol^{-1} determined previously with the flowing-afterglow technique [5] but is lower than the value of -3.3 kcal mol^{-1} that has been determined using high-pressure mass spectrometry [6].

Our values for $\Delta G^0(1)$, $\Delta G^0(2)$ and $\Delta G^0(3)$ indicate the gas-phase basicity order GB(Xe) > GB(SiF_4) > GB(N_2) since ΔG^0 = GB(B_2) − GB(B_1) for reaction 16.

$$B_1H^+ + B_2 \leftrightharpoons B_2H^+ + B_1 \quad (16)$$

Absolute values for gas-phase basicity can be assigned with the choice of a reference value. We have chosen GB(N_2) = 111.0 kcal mol^{-1} as a reference [4] with an uncertainty of ± 1.9 kcal mol^{-1}. This results in a value for GB(SiF_4) = 111.3 ± 2.0 kcal mol^{-1} based on ΔG_1^0, a value of 111.5 ± 2.1 kcal mol^{-1} based on $\Delta G_2^0 - \Delta G_3^0$ and a best estimate of 111.4 ± 1.4 kcal mol^{-1}. This is 2.5 kcal mol^{-1} lower than the currently recommended value of 113.9 kcal mol^{-1} [4].

Gas-Phase Proton Affinities

Proton affinities can be calculated on the basis that $\Delta G_{16}^0 = \Delta H_{16}^0 - T\Delta S_{16}^0$ and that ΔH_{16}^0 = PA(B_2) − PA(B_1). The derived values for ΔH_{16}^0 are included in Table 3. The standard entropy changes were calculated from the entropies of protonation $\Delta S_p^0 \equiv S^0(BH^+) - S^0(B)$ [4]. The reported entropies of protonation of N_2H^+ and XeH^+ are derived from theory and that of SiF_4H^+ was evaluated from the symmetry properties of SiF_4 (T_d, $\sigma = 12$) and SiF_4H^+ (C_s, $\sigma = 1$), where σ is the external symmetry number. The value derived in this way, 4.9 cal mol^{-1} deg^{-1}, is close to the value of 5.25 cal mol^{-1} deg^{-1} we have obtained from theory at B3LYP/6-31+G(d,p). When PA(N_2) = 118.0 ± 1.9 kcal mol^{-1} [4] is chosen as a reference, these results provide a value for PA(SiF_4) = 117.6 ± 2.0 kcal mol^{-1} based on ΔH_1^0, a value of 117.8 ± 2.1 kcal mol^{-1} based on $\Delta H_2^0 - \Delta H_3^0$ and a best estimate of 117.7 ± 1.4 kcal mol^{-1}. This latter value is 2.5 kcal mol^{-1} lower than the currently recommended value for PA(SiF_4) of 120.2 kcal mol^{-1} [4]. The currently recommended value is high because it was based on the value for ΔH_1^0 = 2 kcal mol^{-1} determined in 1984 using FTMS [2]. Our value for ΔH_1^0, − 0.38 ± 0.09 kcal mol^{-1}, is much smaller and negative. According to our results, the order of proton affinities is PA(Xe) > PA(N_2) > PA (SiF_4). As indicated earlier, details on the measured equilibrium constant and the standard entropy change required to calculate ΔPA from the standard free-energy change for reaction 1 were not reported in the previous determination of ΔH_1^0 = 2 kcal mol^{-1} [2] and so it is not possible to make a critical comparison.

Theoretical Results

Results obtained for total energies, scaled zero-point values and thermal corrections for molecules and atoms in their ground-state electronic configurations, are all given in Table 4. Optimized structural details are illustrated in Figure 5 and thermochemical properties at 298 K are given in Table 5. SiF_3^+ is planar with three equal Si–F bonds of 1.538 Å (D_{3h} symmetry). SiF_4 has T_d symmetry with Si–F bonds of 1.579 Å, slightly longer than those in SiF_3^+. The protonation of SiF_4 results in an eclipsed geometry and a dramatic elongation of the Si–F distance to 1.827 Å for the fluorine to which the proton is attached. The other Si–F bond lengths are 1.548 Å and the FSiF angle is 117.2°; both geometric parameters are similar to those in planar SiF_3^+. Thus SiF_4H^+ is essentially SiF_3^+ solvated by a HF molecule, $F_3Si^+ \cdot\cdot HF$. This structure is reminiscent of the structures of analogous HF-solvated species $F_2(OH)Si^+ \cdot\cdot HF$, $F(OH)_2Si^+ \cdot\cdot HF$ and $(OH)_3Si^+ \cdot\cdot HF$ [24], the HF-solvated species

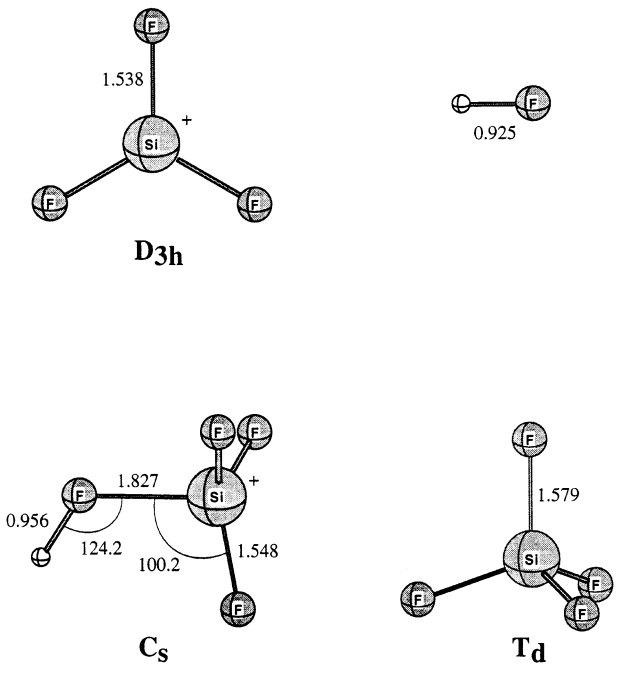

Figure 5. Optimized structures for HF, SiF_3^+, SiF_4, and SiF_4H^+ at B3LYP/6-31+G(d,p).

$F_2(NH_2)Si^+ \cdot\cdot HF$ and $F(NH_2)_2Si^+ \cdot\cdot HF$ [25], and what may be regarded as H_2-solvated species such as SiH_5^+, CH_5^+ and GeH_5^+ [26]. The staggered conformation of SiF_4H^+ was investigated but found to be a transition state and at B3LYP it is 0.2 kcal mol^{-1} above the eclipsed conformation using electronic energies. Inclusion of ZPE and thermal corrections resulted in the transition state being 0.4 kcal mol^{-1} lower in energy than the eclipsed conformation. Effectively there is no barrier to rotation at 298 K.

It is possible to obtain accurate ΔH_f values using high levels of theory [27, 28]. The method we have used here to calculate the standard enthalpies of formation has been described in detail previously [28]. Briefly, the procedure was as follows. The total atomization energy was calculated from the molecular orbital calculations using an isogyric reaction involving H atoms and H_2 to balance the spins [29] and then compensating for the addition of H atoms by using the experimental D_e for H_2 [30]. Inclusion of ZPE then provided D_0 for the molecules. Experimental enthalpies of formation for atoms [31] then enabled us to calculate enthalpies of formation for the molecule. Ions were treated in an identical manner but with an electron being added into the atomization reaction. The stationary electron convention was used. At our highest levels of theory the calculated standard enthalpies of formation for SiF_4 and SiF_4H^+ show considerable variation. At MP4(3df,3pd) our calculated value for $\Delta H_f^0(SiF_4)$ is -376.6 kcal mol^{-1} and the comparable experimental value is close to 10 kcal mol^{-1} different at -386.0 kcal mol^{-1} [4]. There are no experimental values available for comparison of the standard enthalpy of formation SiF_4H^+. The proton affinity of SiF_4 at QCI(3df,3pd) and MP4(3df,3pd) is consistent at 118.7 kcal mol^{-1}. Experience with similar calculations on other chemical systems [32] indicates that these calculations provide values with uncertainties of at least ± 2 kcal mol^{-1} when compared with experimental values.

Table 5. Computed thermochemical properties (in kcal mol^{-1}) at 298 K

	B3LYP[a]	MP4 (2df,p)[b]	QCI (3df,3pd)[c]	MP4 (3df,3pd)[d]
$\Delta H_f^0(SiF_4)$	−354.9	−380.2	−370.9	−376.6
$\Delta H_f^0(SiF_4H^+)$	−111.7	−130.1	−124.0	−129.7
$PA(SiF_4)$	122.6	115.4	118.7	118.7
$D(SiF_3^+ \cdot\cdot HF)$	49.0	39.8	39.6	43.9

[a]Geometry optimization at B3LYP/6-31+G(d,p).
[b]Single-point calculation at MP4SDTQ(fc)/6-311++G(2df,p) using geometries from B3LYP/6-31+G(d,p).
[c]Single-point calculation at QCISD(T)(fc)/6-311++G(3df,3pd) using geometries from B3LYP/6-31+G(d,p).
[d]Single-point calculation at MP4SDTQ(fc)/6-311++G(3df,3pd) using geometries from B3LYP/6-31+G(d,p).

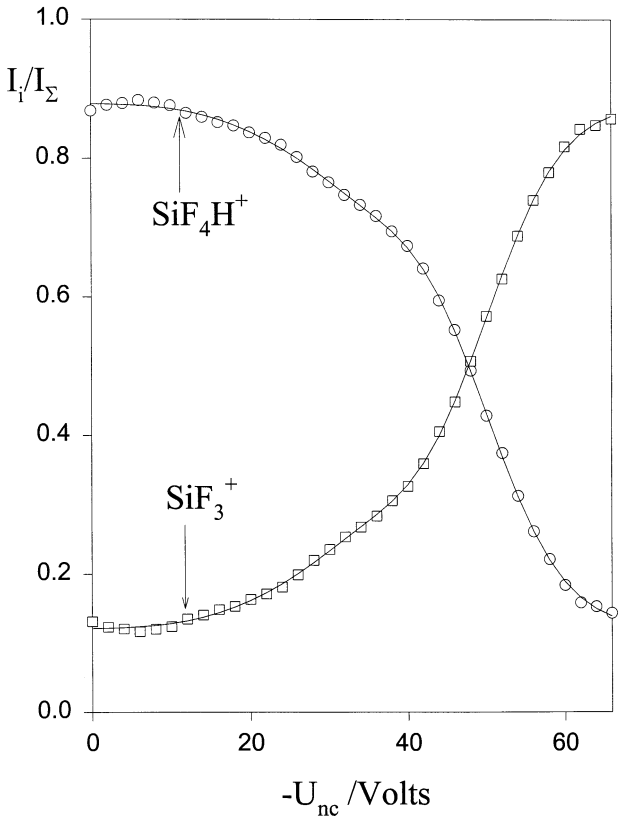

Figure 6. Multi-collision induced dissociation spectrum of SiF_4H^+ in helium buffer gas at 0.35 torr. SiF_4H^+ is formed by the reaction of H_3^+ with SiF_4 at a flow of $SiF_4 = 2.6 \times 10^{17}$ molecules s^{-1}.

CID of SiF_4H^+

The structure of SiF_4H^+ was explored using our SIFT-CID technique [10]. Figure 6 shows the CID spectrum of

SiF_4H^+ produced from the reaction of H_3^+ with SiF_4, reaction 6. The dissociation spectrum is consistent with the structure computed for SiF_4H^+: HF loss is clearly identified. Also, the onset voltage for HF loss is consistent with the computed HF binding energy of 43.9 kcal mol^{-1} at MP4(3df,3pd) judging from the empirical correlation we have established between onset voltage and binding energy [10].

Conclusions

SiF_4 is readily and reversibly protonated in the gas phase. The results of the experimental SIFT measurements and high-level ab initio molecular orbital computations reported in this study indicate that the currently accepted value for PA(SiF_4) is too high by 2.5 kcal mol^{-1} and is within 1 kcal mol^{-1} of the proton affinities of Xe and N_2. The most stable structure of SiF_4H^+ corresponds to a solvated SiF_3^+ core ion and is similar to the structures of the related ions SiH_5^+, CH_5^+ and GeH_5^+.

Acknowledgment

Continued financial support from the Natural Sciences and Engineering Research Council of Canada is much appreciated.

References

1. Senzer, S. N.; Lampe, F. W. *J. Appl. Phys.* **1983,** *54*, 3524–3527.
2. Reents, W. D.; Mujsce, A. M. *Int. J. Mass Spectrom. Ion Processes* **1984,** *59*, 65–75.
3. Lias, S. G.; Liebman, J. F.; Levin, R. D. *J. Phys. Chem. Ref. Data* **1984,** *13*, 695–808.
4. Hunter, E. P.; Lias, S. G. *J. Phys. Chem. Ref. Data* **1998,** *27*, 413–656.
5. Fehsenfeld, F. C.; Lindinger, W.; Schiff, H. I.; Hemsworth, R. S.; Bohme, D. K. *J. Chem. Phys.* **1976,** *64*, 4887–4891.
6. Szulejko, J. E.; McMahon, T. B. *J. Am. Chem. Soc.* **1993,** *115*, 7839–7848.
7. G. I. Mackay, G. I.; Vlachos, G. D.; Bohme, D. K.; Schiff, H. I. *Int. J. Mass Spectrom. Ion Processes* **1980,** *36*, 259–270.
8. Raksit, A. B.; Bohme, D. K. *Int. J. Mass Ion Processes* **1983,** *55*, 69–82.
9. Bohme, D. K.; Hemsworth, R. S.; Rundle, H. W.; Schiff, H. I. *J. Chem. Phys.* **1973,** *58*, 3504–3518.
10. Baranov, V.; Bohme, D. K. *Int. J. Mass Mass Spectrom. Ion Processes* **1996,** *154*, 71–88.
11. Frisch, M. J.; Trucks, G. W.; Schlegel, H. B.; Gill, P. M. W.; Johnson, B. G.; Robb, M. A.; Cheeseman, J. R.; Keith, T.; Petersson, G. A.; Montgomery, J. A.; Raghavachari, K.; Al-Laham, M. A.; Zakrzewski, V. G.; Ortiz, J. V.; Foresman, J. B.; Cioslowski, J.; Stefanov, B. B.; Nanayakkara, A.; Challacombe, M.; Peng, C. Y.; Ayala, P. Y.; Chen, W.; Wong, M. W.; Andres, J. L.; Reploge, E. S.; Gomperts, R.; Martin, R. L.; Fox, D. J.; Binkley, J. S.; DeFrees, D. J.; Baker, J.; Stewart, J. P.; Head-Gordon, M.; Gonzalez, C.; Pople, J. A. GAUSSIAN 94, Revision B.2, Gaussian, Inc., Pittsburgh, PA, 1995.
12. (a) Hohenburg, P.; Kohn, W. *Phys. Rev. B* **1964,** *136*, 864–868. (b) Kohn, W.; Sham, L. J. *Phys. Rev. A* **1965,** *140*, 1133–1141. (c) Salahub, D. R.; Zerner, M. C. *The Challenge of d and f Electrons*; American Chemical Society: Washington, DC, 1989. (d) Parr, R. G.; Yang, W. *Density Functional Theory of Atoms and Molecules*; Oxford Univ. Press: Oxford, UK, 1989. (e) Perdew, J. P.; Chevery, J. A.; Vosko, S. H.; Jackson, K. A.; Pederson, M. R.; Singh, D. J.; Fiolhais, C. *Phys. Rev. B* **1992,** *46*, 6671–6687. (f) Labanowski, J. K.; Andzelm, J. W. *Density Functional Methods in Chemistry*; Springer-Verlag: New York, 1991. (g) Sosa, C.; Lee, C. *J. Chem. Phys.* **1993,** *98*, 8004–8011. (h) Andzelm, J.; Wimmer, E. J. *Chem. Phys.* **1992,** *96*, 1280–1303. (i) Scuseria, G. E. *J. Chem. Phys.* **1992,** *97*, 7528–7530. (j) Becke, A. D. *J. Chem. Phys.* **1992,** *97*, 9173–9177. (k) Becke, A. D. *J. Chem. Phys.* **1992,** *96*, 2155–2160. (l) Gill, P. M. W.; Johnson, B. G.; Pople, J. A.; Frisch, M. J. *Chem. Phys. Lett.* **1992,** *197*, 499–505. (m) Stephens, P. J.; Devlin, F. J.; Chabalowski, C. F.; Frisch, M. J. *J. Phys. Chem.* **1994,** *98*, 11623–11627.
13. Slater, J. C. *Quantum Theory of Molecules and Solids, Vol. 4: The Self-Consistent Field for Molecules and Solids*; McGraw-Hill: New York, 1974.
14. Becke, A. D. *Phys. Rev. A* **1998,** *38*, 3098–3100.
15. Lee, C.; Yang, W.; Parr, R. G. *Phys. Rev. B* **1988,** *37*, 785–789.
16. Miehlich, B.; Savin, A.; Stoll, H.; Preuss, H. *Chem. Phys. Lett.* **1989,** *157*, 200–206.
17. (a) Ditchfield, R.; Hehre, W. J.; Pople, J. A. *J. Chem. Phys.* **1971,** *54*, 724–728. (b) Chandrasekhar, J.; Andrade, J. G.; Schleyer, P.v.R. *J. Am. Chem. Soc.* **1981,** *103*, 5609–5612. (c) Chandrasekhar, J.; Spitznagel, G. W. Schleyer, P.v.R. *J. Comput. Chem.* **1983,** *4*, 294–301. (d) Hariharan, P. C.; Pople, J. A. *Chem. Phys. Lett.* **1972,** *16*, 217–219.
18. Møller, C.; Plesset, M. S. *Phys. Rev.* **1934,** *45*, 618–623.
19. Frisch, M.; Pople, J. A.; Binkley, J. S. *J. Chem. Phys.* **1984,** *80*, 3265–3269.
20. Pople, J. A.; Head-Gordon, M.; Raghavachari, K. *J. Chem. Phys.* **1987,** *87*, 5968–5975.
21. Gioumousis, G.; Stevenson, D. P. *J. Chem. Phys.* **1958,** *29*, 294–299.
22. Cipollini, R.; Grandinetti, F. *J. Chem. Soc. Commun.* **1995,** *7*, 773–774.
23. (a) Kickel, B. L.; Fisher, E. R.; Armentrout, P. B. *J. Phys. Chem.* **1993,** *97*, 10198–10203. (b) Fisher, E. R.; Kickel, B. L.; Armentrout, P. B. *J. Phys. Chem.* **1993,** *97*, 10204–10210.
24. Ketvirtis, A. E.; Baranov, V. I.; Hopkinson, A. C.; Bohme, D. K. *J. Phys. Chem.* **1998,** *102*, 1162–1169.
25. Ketvirtis, A. E.; Baranov, V. I.; Ling, Y.; Hopkinson, A. C.; Bohme, D. K. *Int. J. Mass Spectrom.* **1999,** *185/186/187*, 381–392.
26. See, for example, Schreiner, P. R.; Schaefer, H. F.; v. Ragué Schleyer, P. *Adv. Gas Phase Ion Chem.* **1996,** *2*, 125–160.
27. Chase, M. W.; Davies, C. A.; Downey, J. R.; Frurip, D. J.; McDonald, R. A.; Syverud, A. N. JANAF Thermochemical Tables, 3rd ed., *J. Phys. Chem. Ref. Data* **1985,** *14*.
28. (a) Rodriquez, C. F.; Sirois, S.; Hopkinson, A. C. *J. Org. Chem.* **1992,** *57*, 4869–4876. (b) Rodriquez, C. F.; Bohme, D. K.; Hopkinson, A. C. *J. Phys. Chem.* **1996,** *100*, 2942–2949.
29. (a) Rodriquez, C. F.; Hopkinson, A. C. *J. Phys. Chem.* **1993,** *97*, 849–855. (b) Rodriquez, C. F.; Bohme, D. K.; Hopkinson, A. C. *J. Org. Chem.* **1993,** *58*, 3344–3349.
30. (a) Pople, J. A.; Luke, B. T.; Frisch, M. J.; Binkley, J. S. *J. Phys. Chem.* **1985,** *89*, 2198–2203. (b) Curtiss, L. A.; Pople, J. A. *J. Phys. Chem.* **1987,** *91*, 155–162. (c) Pople, J. A.; Curtiss, L. A. *J. Phys. Chem.* **1987,** *91*, 3637–3639. (d) Curtiss, L. A.; Raghavachari, K.; Pople, J. A. *Chem. Phys. Lett.* **1993,** *214*, 183–185.
31. Kolos, W.; Wolniewiecz, L. *J. Chem. Phys.* **1968,** *49*, 404–410.
32. (a) Del Bene, J. E.; Shavitt, I. *J. Phys. Chem.* **1990,** *94*, 5514–5518. (b) DeFrees, D. J.; McLean, A. D. *J. Comput. Chem.* **1986,** *7*, 321–333.